Geodesics in Heat: A New Approach to Computing Distance Based on Heat Flow

KEENAN CRANE
Caltech
CLARISSE WEISCHEDEL, MAX WARDETZKY
University of Göttingen

We introduce the *heat method* for computing the geodesic distance to a specified subset (*e.g.*, point or curve) of a given domain. The heat method is robust, efficient, and simple to implement since it is based on solving a pair of standard linear elliptic problems. The resulting systems can be prefactored once and subsequently solved in near-linear time. In practice, distance is updated an order of magnitude faster than with state-of-the-art methods, while maintaining a comparable level of accuracy. The method requires only standard differential operators and can hence be applied on a wide variety of domains (grids, triangle meshes, point clouds, *etc.*). We provide numerical evidence that the method converges to the exact distance in the limit of refinement; we also explore smoothed approximations of distance suitable for applications where greater regularity is required.

Categories and Subject Descriptors: I.3.5 [**Computer Graphics**]: Computational Geometry and Object Modeling—*Geometric algorithms, languages, and systems*

General Terms: Algorithms

Additional Key Words and Phrases: digital geometry processing, discrete differential geometry, geodesic distance, distance transform, heat kernel

ACM Reference Format:

Keenan Crane, Clarisse Weischedel, and Max Wardetzky. 2013. Geodesics in Heat: A New Approach to Computing Distance Based on Heat Flow. *ACM Trans. Graph.* 28, 4, Article 106 (September 2009), 10 pages.
DOI: http://dx.doi.org/10.1145/XXXXXXX.YYYYYYY

1. INTRODUCTION

Imagine touching a scorching hot needle to a single point on a surface. Over time heat spreads out over the rest of the domain and can be described by a function $k_{t,x}(y)$ called the *heat kernel*, which measures the heat transferred from a source x to a destination y after time t. A well-known relationship between heat and distance is Varadhan's formula [1967], which says that the geodesic distance ϕ between any pair of points x, y on a Riemannian manifold can be recovered via a simple pointwise transformation of the heat kernel:

$$\phi(x, y) = \lim_{t \to 0} \sqrt{-4t \log k_{t,x}(y)}. \tag{1}$$

The intuition behind this behavior stems from the fact that heat diffusion can be modeled as a large collection of hot particles taking random walks starting at x: any particle that reaches a distant point y after a small time t has had little time to deviate from the shortest possible path. To date, however, this relationship has not been exploited by numerical algorithms that compute geodesic distance.

Why has Varadhan's formula been overlooked in this context? The main reason, perhaps, is that it requires a precise numerical reconstruction of the heat kernel, which is difficult to obtain – applying the formula to a mere approximation of $k_{t,x}$ does not yield the correct result, as illustrated in Figures 2 and 6. The heat method circumvents this issue by working with a broader class of inputs, namely any function whose gradient is parallel to geodesics. We can then separate computation into two stages: first find the gradient of the distance field, then recover the distance itself.

Relative to existing algorithms, the heat method offers two major advantages. First, it can be applied to virtually any type of geometric discretization, including regular grids, polygonal meshes, and even unstructured point clouds. Second, it involves only sparse linear systems, which can be prefactored once and rapidly re-solved many times. This feature makes the heat method particularly valuable for applications such as shape matching, path planning, and level set-based simulation (*e.g.*, free-surface fluid flows), which require repeated distance queries on a fixed geometric domain. Moreover, because linear elliptic equations are widespread in scientific computing, the heat method can immediately take advantage of new developments in numerical linear algebra and parallelization.

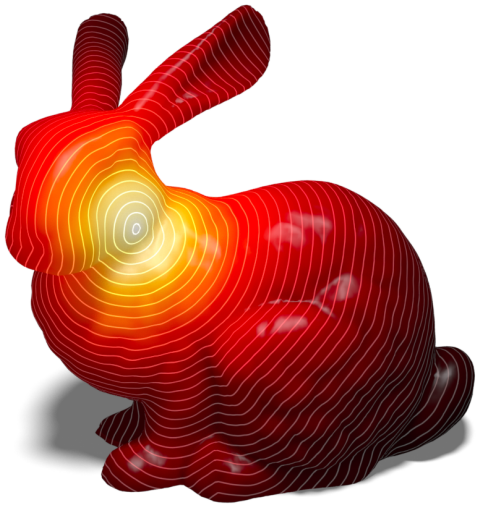

Fig. 1. Geodesic distance from a single point on a surface. The heat method allows distance to be rapidly updated for new source points or curves.
Bunny mesh courtesy Stanford Computer Graphics Laboratory.

DOI: http://dx.doi.org/10.1145/XXXXXXX.YYYYYYY

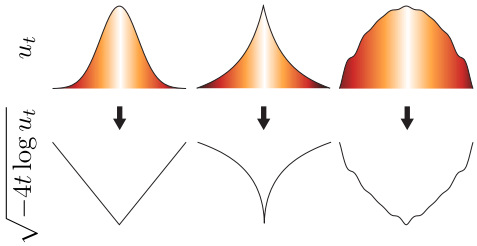

Fig. 2. Given an *exact* reconstruction of the heat kernel *(top left)* Varadhan's formula can be used to recover geodesic distance *(bottom left)* but fails in the presence of approximation or numerical error *(middle, right)*, as shown here for a point source in 1D. The robustness of the heat method stems from the fact that it depends only on the *direction* of the gradient.

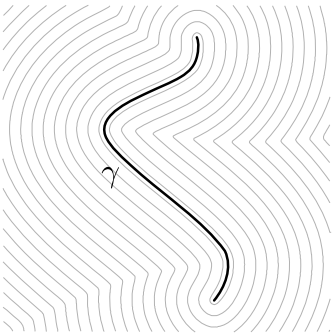

Fig. 3. The heat method computes the shortest distance to a subset γ of a given domain. Gray curves indicate isolines of the distance function.

2. RELATED WORK

The prevailing approach to distance computation is to solve the *eikonal equation*

$$|\nabla \phi| = 1 \tag{2}$$

subject to boundary conditions $\phi|_\gamma = 0$ over some subset γ of the domain. This formulation is *nonlinear* and *hyperbolic*, making it difficult to solve directly. Typically one applies an iterative relaxation scheme such as Gauss-Seidel – special update orders are known as *fast marching* and *fast sweeping*, which are some of the most popular algorithms for distance computation on regular grids [Sethian 1996] and triangulated surfaces [Kimmel and Sethian 1998]. These algorithms can also be used on implicit surfaces [Memoli and Sapiro 2001], point clouds [Memoli and Sapiro 2005], and polygon soup [Campen and Kobbelt 2011], but only indirectly: distance is computed on a simplicial mesh or regular grid that approximates the original domain. Implementation of fast marching on simplicial grids is challenging due to the need for nonobtuse triangulations (which are notoriously difficult to obtain) or else a complex unfolding procedure to preserve monotonicity of the solution; moreover these issues are not well-studied in dimensions greater than two. Fast marching and fast sweeping have asymptotic complexity of $O(n \log n)$ and $O(n)$, respectively, but sweeping is often slower due to the large number of sweeps required to obtain accurate results [Hysing and Turek 2005].

The main drawback of these methods is that they do not reuse information: the distance to different subsets γ must be computed entirely from scratch each time. Also note that both sweeping and marching present challenges for parallelization: priority queues are inherently serial, and irregular meshes lack a natural sweeping order. Weber *et al.* [2008] address this issue by decomposing surfaces into regular grids, but this decomposition resamples the surface and requires a low-distortion parameterization over a small number of quadrilateral patches, which is difficult to obtain.

In a different development, Mitchell *et al.* [1987] give an $O(n^2 \log n)$ algorithm for computing the exact polyhedral distance from a single source to all other vertices of a triangulated surface. Surazhsky *et al.* [2005] demonstrate that this algorithm tends to run in sub-quadratic time in practice, and present an approximate $O(n \log n)$ version of the algorithm with guaranteed error bounds; Bommes and Kobbelt [2007] extend the algorithm to polygonal sources. Similar to fast marching, these algorithms propagate distance information in wavefront order using a priority queue, again making them difficult to parallelize. More importantly, the amortized cost of these algorithms (over many different source subsets γ) is substantially greater than for the heat method since they do not reuse information from one subset to the next. Finally, although [Surazhsky et al. 2005] greatly simplifies the original formulation, these algorithms remain challenging to implement and do not immediately generalize to domains other than triangle meshes.

Closest to our approach is the recent method of Rangarajan and Gurumoorthy [2011], who do not appear to be aware of Varadahn's formula – they instead derive an analogous relationship $\phi = -\sqrt{\hbar \log \psi}$ between the distance function and solutions ψ to the time-independent Schrödinger equation. We emphasize, however, that this derivation applies only in $\mathbb{R}^n$ where ψ takes a special form – in this case it may be just as easy to analytically invert the Euclidean heat kernel $u_{t,x} = (4\pi t)^{-n/2} e^{-\phi(x,y)^2/4t}$. Moreover, they compute solutions using the fast Fourier transform, which limits its computation to regular grids. To obtain accurate results their method requires either the use of arbitrary-precision arithmetic or a combination of multiple solutions for various values of $\hbar$; no general guidance is provided for determining appropriate values of $\hbar$.

Finally, there is a large literature on *smoothed distances* [Coifman and Lafon 2006; Fouss et al. 2007; Rustamov et al. 2009; Lipman et al. 2010], which are valuable in contexts where differentiability is required. However, existing smooth distances may not be appropriate in contexts where the *geometry* of the original domain is important, since they do not attempt to approximate the original metric and therefore substantially violate the unit-speed nature of geodesics (Figure 10). These distances also have an interpretation in terms of simple discretizations of heat flow – see Section 3.3 for further discussion.

Fig. 4. Distance to the boundary on a region in the plane (left) or a surface in $\mathbb{R}^3$ is achieved by simply placing heat along the boundary curve. Note good recovery of the *cut locus*, *i.e.*, points with more than one closest point on the boundary.

Car mesh courtesy AIM@Shape.

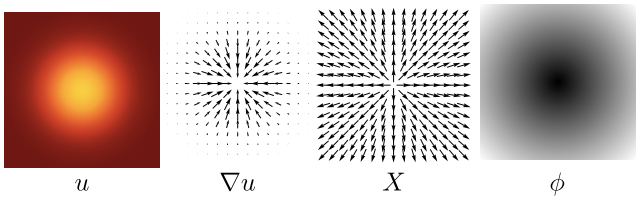

Fig. 5. Outline of the heat method. (I) Heat u is allowed to diffuse for a brief period of time *(left)*. (II) The temperature gradient ∇u *(center left)* is normalized and negated to get a unit vector field X *(center right)* pointing along geodesics. (III) A function ϕ whose gradient follows X recovers the final distance *(right)*.

3. THE HEAT METHOD

Our method can be described purely in terms of operations on smooth manifolds; we explore spatial and temporal discretization in Sections 3.1 and 3.2, respectively. Let Δ be the negative-semidefinite Laplace–Beltrami operator acting on (weakly) differentiable real-valued functions over a Riemannian manifold (M, g). The heat method consists of three basic steps:

Algorithm 1 The Heat Method

I. Integrate the heat flow $\dot{u} = \Delta u$ for some fixed time t.
II. Evaluate the vector field $X = -\nabla u / |\nabla u|$.
III. Solve the Poisson equation $\Delta \phi = \nabla \cdot X$.

The function ϕ approximates geodesic distance, approaching the true distance as t goes to zero (Eq. (1)). Note that the solution to step III is unique only up to an additive constant – final values simply need to be shifted such that the smallest distance is zero. Initial conditions $u_0 = \delta(x)$ (*i.e.*, a Dirac delta) recover the distance to a single source point $x \in M$ as in Figure 1, but in general we can compute the distance to any piecewise submanifold γ by setting u_0 to a generalized Dirac [Villa 2006] over γ (see Figures 3 and 4).

The heat method can be motivated as follows. Consider an approximation u_t of heat flow for a fixed time t. Unless u_t exhibits *precisely* the right rate of decay, Varadhan's transformation $u_t \mapsto \sqrt{-4t \log u_t}$ will yield a poor approximation of the true geodesic distance ϕ because it is highly sensitive to errors in magnitude (see Figures 2 and 6). The heat method asks for something different: it asks only that the gradient ∇u_t points in the right direction, *i.e.*, parallel to $\nabla \phi$. Magnitude can safely be ignored since we know (from the eikonal equation) that the gradient of the true distance function has unit length. We therefore compute the normalized gradient field $X = -\nabla u / |\nabla u|$ and find the closest scalar potential ϕ by minimizing $\int_M |\nabla \phi - X|^2$, or equivalently, by solving the corresponding Euler-Lagrange equations $\Delta \phi = \nabla \cdot X$ [Schwarz 1995]. The overall procedure is depicted in Figure 5.

3.1 Time Discretization

We discretize the heat equation from step I of Algorithm 1 in time using a single backward Euler step for some fixed time t. In practice, this means we simply solve the linear equation

$$(\mathrm{id} - t\Delta) u_t = u_0 \tag{3}$$

over the entire domain M, where id is the identity (here we still consider a smooth manifold; spatial discretization is discussed in Section 3.2). We can get a better understanding of solutions to Eq. (3) by considering the elliptic boundary value problem

$$\begin{aligned} (\mathrm{id} - t\Delta) v_t &= 0 \quad \text{on} \quad M \backslash \gamma \\ v_t &= 1 \quad \text{on} \quad \gamma\,. \end{aligned} \tag{4}$$

which for a point source yields a solution v_t equal to u_t up to a multiplicative constant. As established by Varadhan in his proof of Eq. (1), v_t also has a close relationship with distance, namely

$$\lim_{t \to 0} -\tfrac{\sqrt{t}}{2} \log v_t = \phi \tag{5}$$

away from the cut locus. This relationship ensures the validity of steps II and III since the transformation applied to v_t preserves the direction of the gradient.

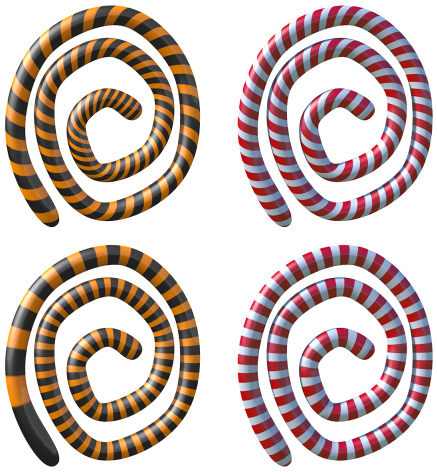

Fig. 6. *Left:* Varadhan's formula. *Right:* the heat method. Even for very small values of t, simply applying Varadhan's formula does not provide an accurate approximation of geodesic distance *(top left)*; for large values of t spacing becomes even more uneven *(bottom left)*. Normalizing the gradient results in a more accurate solution, as indicated by evenly spaced isolines *(top right)*, and is also valuable when constructing a smoothed distance function *(bottom right)*.

3.2 Spatial Discretization

In principle the heat method can be applied to any domain with a discrete gradient (∇), divergence ($\nabla \cdot$) and Laplace operator (Δ). Note that these operators are highly local and hence do not exhibit significant cancellation error despite large global variation in u_t.

3.2.1 *Simplicial Meshes.* Let $u \in \mathbb{R}^{|V|}$ specify a piecewise linear function on a triangulated surface. A standard discretization of the Laplacian at a vertex i is given by

$$(Lu)_i = \frac{1}{2A_i} \sum_j (\cot \alpha_{ij} + \cot \beta_{ij})(u_j - u_i),$$

where A_i is one third the area of all triangles incident on vertex i, the sum is taken over all neighboring vertices j, and α_{ij}, β_{ij} are the angles opposing the corresponding edge [MacNeal 1949]. We can express this operation via a matrix $L = A^{-1} L_C$, where $A \in \mathbb{R}^{|V| \times |V|}$ is a diagonal matrix containing the vertex areas and $L_C \in \mathbb{R}^{|V| \times |V|}$ is

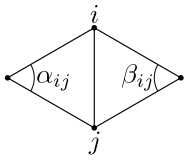

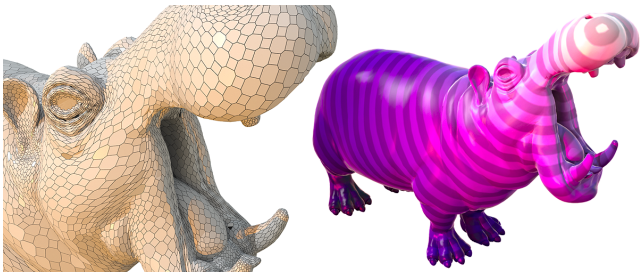

Fig. 7. Since the heat method is based on well-established discrete operators like the Laplacian, it is easy to adapt to a variety of geometric domains. Above: distance on a hippo composed of high-degree nonplanar (and sometimes nonconvex) polygonal faces.

Hippo mesh courtesy Luxology LLC.

the *cotan operator* representing the remaining sum. Heat flow can then be computed by solving the symmetric positive-definite system

$$(A - tL_C)u = \delta_\gamma$$

where δ_γ is a Kronecker delta over γ (the mass matrix A need not appear on the right-hand side – a Kronecker delta already gives the integrated value of a Dirac delta). The gradient in a given triangle can be expressed succinctly as

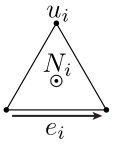

$$\nabla u = \frac{1}{2A_f} \sum_i u_i (N \times e_i)$$

where A_f is the area of the face, N is its unit normal, e_i is the ith edge vector (oriented counterclockwise), and u_i is the value of u at the opposing vertex. The integrated divergence associated with vertex i can be written as

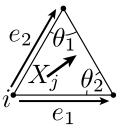

$$\nabla \cdot X = \frac{1}{2} \sum_j \cot\theta_1 (e_1 \cdot X_j) + \cot\theta_2 (e_2 \cdot X_j)$$

where the sum is taken over incident triangles j each with a vector X_j, e_1 and e_2 are the two edge vectors of triangle j containing i, and θ_1, θ_2 are the opposing angles. If we let $b \in \mathbb{R}^{|V|}$ be the vector of (integrated) divergences of the normalized vector field X, then the final distance function is computed by solving the symmetric Poisson problem

$$L_C \phi = b.$$

Conveniently, this discretization easily generalizes to higher dimensions (*e.g.*, tetrahedral meshes) using well-established discrete operators; see for instance [Desbrun et al. 2008].

3.2.2 *Polygonal Surfaces.* For a mesh with (not necessarily planar) polygonal faces, we use the polygonal Laplacian defined by Alexa and Wardetzky [2011]. The only difference in this setting is that the gradient of the heat kernel is expressed as a discrete 1-form associated with half edges, hence we cannot directly evaluate the magnitude of the gradient $|\nabla u|$ needed for the normalization step (Algorithm 1, step II). To resolve this issue we assume that ∇u is constant over each face, implying that

$$u_f^T L_f u_f = \int_M |\nabla u|^2 dA = |\nabla u|^2 A_f,$$

where u_f is the vector of heat values in face f, A_f is the magnitude of the area vector, and L_f is the local (weak) Laplacian. We can

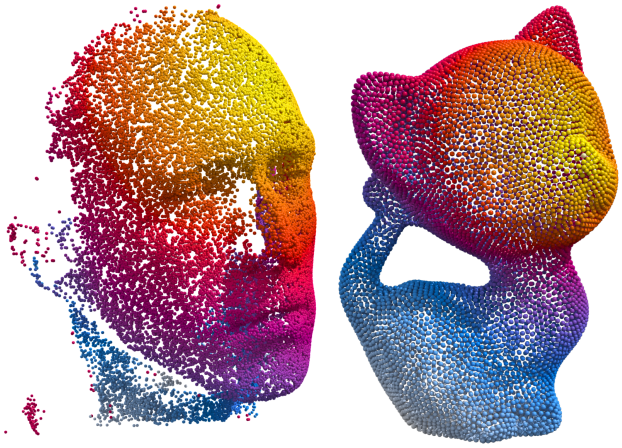

Fig. 8. The heat method can be applied directly to point clouds that lack connectivity information. *Left:* face scan with holes and noise. *Right:* kitten surface with connectivity removed. Yellow points are close to the source; disconnected clusters (in the sense of Liu *et al.*) receive a constant red value.

Kitten mesh courtesy AIM@Shape.

therefore approximate the magnitude of the gradient as

$$|\nabla u|_f = \sqrt{\frac{u_f^T L_f u_f}{A_f}}.$$

This quantity is used to normalize the 1-form values associated with half edges in the corresponding face. The integrated divergence is then given by $\mathrm{d}^T M \alpha$ where α is the normalized gradient, d is the coboundary operator and M is the mass matrix for 1-forms (see [Alexa and Wardetzky 2011] for details). These operators are applied in steps I-III as usual. Figure 7 demonstrates distance computed on an irregular polygonal mesh.

3.2.3 *Point Clouds.* For a discrete point sample $P \subset \mathbb{R}^n$ of M with no connectivity information, we solve the heat equation (step I) using the *point cloud* Laplacian recently introduced by Liu et al. [2012], which extends previous work of Belkin et al. [2009a]. In this formulation, the Laplacian is represented by $A_V^{-1} L_{PC}$, where A_V is a diagonal matrix of Voronoi areas and L_{PC} is symmetric positive semidefinite (see [Liu et al. 2012], Section 3.4, for details).

To compute the vector field $X = -\nabla u / |\nabla u|$ (step II), we represent the function $u : P \to \mathbb{R}$ as a height function over approximate tangent planes T_p at each point $p \in P$ and evaluate the gradient of a weighted least squares (WLS) approximation of u [Nealen 2004]. This approximation provides a discrete gradient operator $D \in \mathbb{R}^{|P|\times|P|}$. To compute tangent planes, we use a moving least squares (MLS) approximation for simplicity, although other choices are possible (see Liu *et al.*). To find the best-fit scalar potential ϕ (step III), we solve the linear, positive-semidefinite Poisson equation $L_{PC}\phi = D^T A_V X$. Figure 8 shows two examples.

Other discretizations are certainly possible (see for instance [Luo et al. 2009]); we picked one that was simple to implement in any dimension. Note that the computational cost of the heat method depends primarily on the *intrinsic* dimension n of M, whereas methods based on fast marching require a grid of the same dimension m as the ambient space [Memoli and Sapiro 2001] – this distinction is especially important in contexts like machine learning where m may be significantly larger than n.

3.2.4 *Choice of Time Step.* Accuracy of the heat method relies in part on the time step t. In the smooth setting, Eq. (5) suggests that smaller values of t yield better approximations of geodesic distance. In the discrete setting we instead discover that the limit solution to Eq. (3) is purely a function of the *combinatorial* distance, independent of how we discretize the Laplacian (see Appendix A). Therefore, on a *fixed* mesh decreasing the value of t does not necessarily improve accuracy, even in exact arithmetic. (Of course, we can always improve accuracy by refining the mesh and decreasing t accordingly.) Moreover, large values of t produce a smoothed approximation of geodesic distance (Section 3.3). We therefore seek an optimal time step t^* that is neither too large nor too small.

Determining a provably optimal expression for t^* is difficult due to the complexity of analysis involving the cut locus [Neel and Stroock 2004]. We instead use a simple estimate that works remarkably well in practice, namely $t = mh^2$ where h is the mean spacing between adjacent nodes and $m > 0$ is a constant. This estimate is motivated by the fact that $h^2\Delta$ is invariant with respect to scale and refinement; experiments on a regular grid (Figure 18) suggest that $m = 1$ is the smallest parameter value that recovers the ℓ_2 distance, and indeed this value yields near-optimal accuracy for a wide variety of irregularly triangulated surfaces, as demonstrated in Figure 20. In this paper the time step

$$\boxed{t = h^2}$$

is therefore used uniformly throughout all tests and examples, except where we explicitly seek a smoothed approximation of distance, as in Section 3.3. For highly nonuniform meshes one could set h to the *maximum* spacing, providing a more conservative estimate. Numerical underflow could theoretically occur for extremely small t, though we do not encounter this issue in practice.

3.3 Smoothed Distance

Geodesic distance fails to be smooth at points in the *cut locus*, *i.e.*, points at which there is no unique shortest path to the source – these points appear as sharp cusps in the level lines of the distance function. Non-smoothness can result in numerical difficulty for applications which need to take derivatives of the distance function ϕ (*e.g.*, level set methods), or may simply be undesirable aesthetically.

Several distances have been designed with smoothness in mind, including diffusion distance [Coifman and Lafon 2006], commute-time distance [Fouss et al. 2007], and biharmonic distance [Lipman et al. 2010] (see the last reference for a more detailed discussion). These distances satisfy a number of important properties (smoothness, isometry-invariance, *etc.*), but are poor approximations of true geodesic distance, as indicated by uneven spacing of isolines (see Figure 10, middle). They can also be expensive to evaluate, requiring either a large number of Laplacian eigenvectors ($\sim 150 - 200$ in practice) or the solution to a linear system at each vertex.

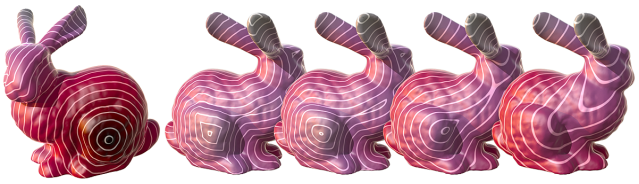

Fig. 9. A source on the front of the Stanford Bunny results in nonsmooth cusps on the opposite side. By running heat flow for progressively longer durations t, we obtain smoothed approximations of geodesic distance *(right)*.
Bunny mesh courtesy Stanford Computer Graphics Laboratory.

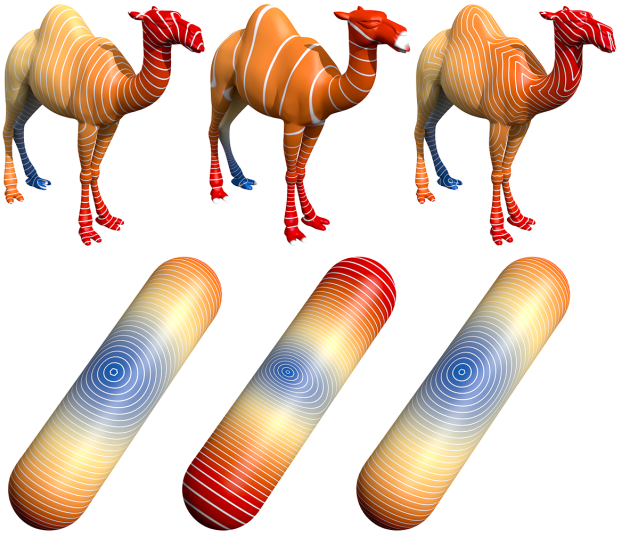

Fig. 10. *Top row:* our smoothed approximation of geodesic distance (left) and biharmonic distance (center) both mitigate sharp "cusps" found in the exact distance (right), yet isoline spacing of the biharmonic distance can vary dramatically. Bottom row: biharmonic distance (center) tends to exhibit elliptical level lines near the source, while our smoothed distance (left) maintains isotropic circular profiles as seen in the exact distance (right).
Camel mesh courtesy AIM@Shape.

In contrast, one can rapidly construct smoothed approximations of geodesic distance by simply applying the heat method for large values of t (Figure 9). The computational cost remains the same, and isolines are evenly spaced for any value of t due to normalization (step II); the solution is isometrically invariant since it depends only on intrinsic differential operators. For a time step $t = mh^2$, meaningful values of m are found in the range $1 - 10^6$ – past this point the term $t\Delta$ dominates, resulting in little visible change.

Existing smooth distance functions can also be understood in terms of time-discrete heat flow. In particular, the commute-time distance d_C and biharmonic distance d_B can be expressed in terms of the harmonic and biharmonic Green's functions g_C and g_B:

$$\begin{aligned} d_C(x,y)^2 &= g_C(x,x) - 2g_C(x,y) + g_C(y,y), \\ d_B(x,y)^2 &= g_B(x,x) - 2g_B(x,y) + g_B(y,y). \end{aligned}$$

On a manifold of constant sectional curvature the sum $g(x,x) + g(y,y)$ is constant. Locally, then, commute-time and biharmonic distance look like the harmonic and biharmonic Green's functions (respectively), which can be expressed via one- and two-step backward Euler approximations of heat flow:

$$\begin{aligned} g_C &= \lim_{t\to\infty}(\mathrm{id} - t\Delta)^\dagger\delta, \\ g_B &= \lim_{t\to\infty}(\mathrm{id} - 2t\Delta + t^2\Delta^2)^\dagger\delta. \end{aligned}$$

(Here $\dagger$ denotes the pseudoinverse.)

3.4 Boundary Conditions

When computing the exact distance, either vanishing Neumann or Dirichlet conditions suffice since this choice does not affect the behavior of the smooth limit solution (see [von Renesse 2004], Corollary 2 and [Norris 1997], Theorem 1.1, respectively). Boundary conditions do however alter the behavior of our smoothed distance. Although there is no well-defined "correct" behavior for this smoothed function, we advocate the use of *averaged* boundary con-

Fig. 11. Effect of Neumann (top-left), Dirichlet (top-right) and averaged (bottom-left) boundary conditions on smoothed distance. Averaged boundary conditions mimic the behavior of the same surface without boundary.

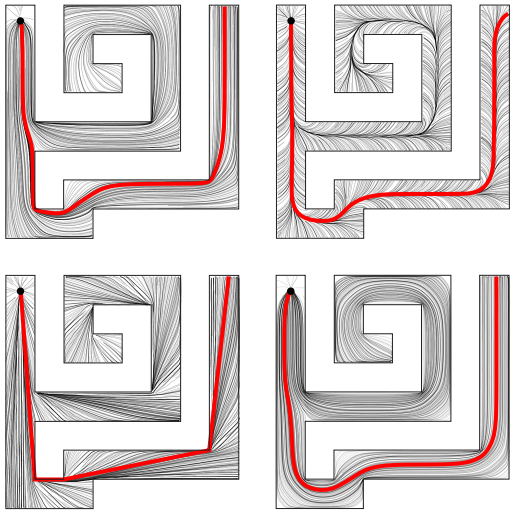

Fig. 12. For path planning, the behavior of geodesics can be controlled via boundary conditions and the time step t. *Top-left:* Neumann conditions encourage boundary adhesion. *Top-right:* Dirichlet conditions encourage avoidance. *Bottom-left:* small values of t yield standard straight-line geodesics. *Bottom-right:* large values of t yield more natural trajectories.

ditions obtained by taking the mean of the Neumann solution u_N and the Dirichlet solution u_D, *i.e.*, $u = \frac{1}{2}(u_N + u_D)$. These conditions tend to produce isolines that are not substantially influenced by the shape of the boundary (Figures 11 and 19). The intuition behind this behavior again stems from a random walker interpretation: zero Dirichlet conditions absorb heat, causing walkers to "fall off" the edge of the domain. Neumann conditions prevent heat from flowing out of the domain, effectively "reflecting" random walkers. Averaged conditions mimic the behavior of a domain without boundary: the number of walkers leaving equals the number of walkers returning. Figure 12 shows how boundary conditions affect the behavior of geodesics in a path-planning scenario.

4. EVALUATION

4.1 Performance

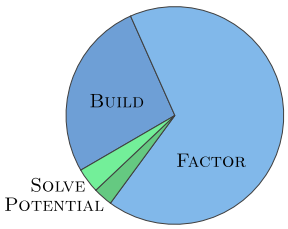

A key advantage of the heat method is that the linear systems in steps (I) and (III) can be prefactored. Our implementation uses sparse Cholesky factorization [Chen et al. 2008], which for Poisson-type problems has guaranteed sub-quadratic complexity but in practice scales even better [Botsch et al. 2005]; moreover there is strong evidence to suggest that sparse systems arising from elliptic PDEs can be solved in very close to linear time [Schmitz and Ying 2012; Spielman and Teng 2004]. Independent of these issues, the amortized cost for problems with a large number of right-hand sides is roughly linear, since back substitution can be applied in essentially linear time. See inset for a breakdown of relative costs in our implementation.

In terms of absolute performance, a number of factors affect the run time of the heat method including the spatial discretization, choice of discrete Laplacian, geometric data structures, and so forth. As a typical example, we compared our simplicial implementation (Section 3.2.1) to the first-order fast marching method of Kimmel & Sethian [1998] and the exact algorithm of Mitchell *et al.* [1987] as described by Surazhsky *et al.* [2005]. In particular we used the state-of-the-art fast marching implementation of Peyré and Cohen [2005] and the exact implementation of Kirsanov [Surazhsky et al. 2005]. The heat method was implemented in ANSI C in double precision using a simple vertex-face adjacency list. Performance was measured using a single core of a 2.4 GHz Intel Core 2 Duo (Table I). Note that even for a single distance computation the heat method outperforms fast marching; more importantly, updating distance for new subsets γ is consistently an order of magnitude faster (or more) than both fast marching and the exact algorithm.

4.2 Accuracy

We examined errors in the heat method, fast marching [Kimmel and Sethian 1998], and the polyhedral distance [Mitchell et al. 1987], relative to mean edge length h on triangulated surfaces. Figures 21 and 22 illustrate convergence on simple geometries where the exact distance can be easily obtained. Both fast marching and the heat method appear to exhibit linear convergence; it is interesting to note that even the exact *polyhedral* distance provides only quadratic convergence. Keeping this fact in mind, Table I uses the polyhedral distance as a baseline for comparison on more complicated geometries – MAX is the maximum error as a percentage of mesh diameter and MIN is the mean relative error at each vertex (a convention introduced in [Surazhsky et al. 2005]). Note that fast marching tends to achieve a smaller maximum error, whereas the heat method does better on average. Figure 14 gives a visual comparison of accuracy; the only notable discrepancy is a slight smoothing at sharp cusps, which may explain the slightly larger maximum error exhibited by the heat method. Figure 15 indicates that this phenomenon does not interfere with the extraction of the cut locus – here we simply visualize values of $|\Delta\phi|$ above a fixed threshold. Figure 23 plots the maximum violation of metric properties – both the heat method and fast marching exhibit small approximation errors that vanish under refinement. Even for smoothed distance ($m \gg 1$) the triangle inequality is violated only for highly degenerate geodesic triangles, *i.e.*, all three points on a common geodesic. In contrast, smoothed distances discussed in Section 2 satisfy metric properties exactly,

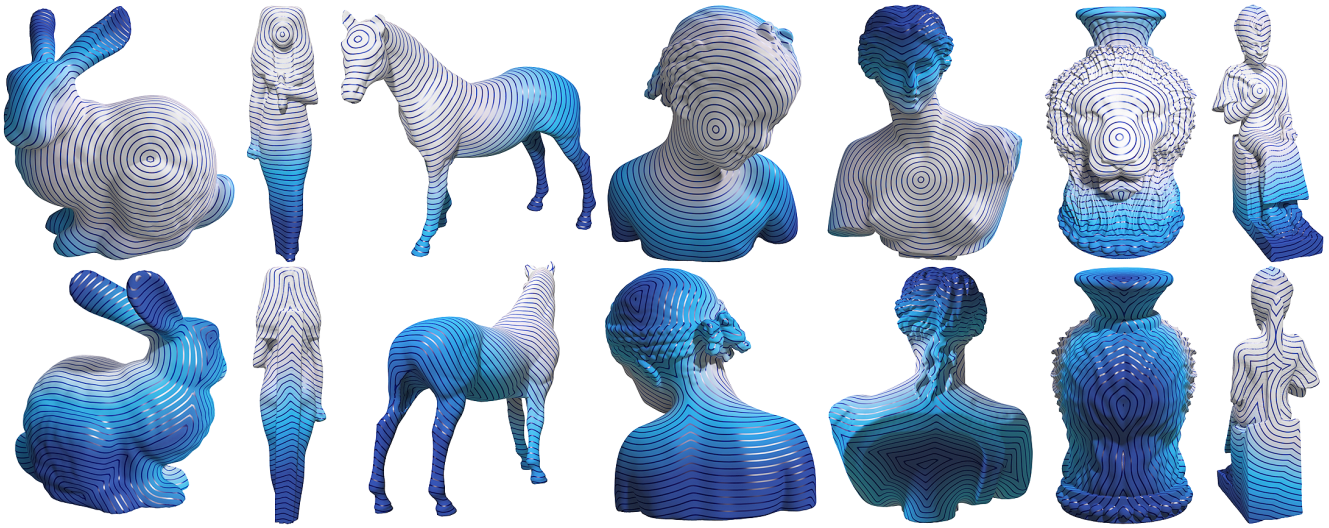

Fig. 13. Meshes used in Table I. Left to right: BUNNY, ISIS, HORSE, BIMBA, APHRODITE, LION, RAMSES[1].

Table I. Comparison with fast marching and exact polyhedral distance. Best speed/accuracy in **bold**; speedup in **orange**.

MODEL	TRIANGLES	HEAT METHOD				FAST MARCHING			EXACT
		PRECOMPUTE	SOLVE	MAX ERROR	MEAN ERROR	TIME	MAX ERROR	MEAN ERROR	TIME
BUNNY	28k	**0.21s**	**0.01s (28x)**	3.22%	**1.12%**	0.28s	**1.06%**	1.15%	0.95s
ISIS	93k	**0.73s**	**0.05s (21x)**	1.19%	**0.55%**	1.06s	**0.60%**	0.76%	5.61s
HORSE	96k	**0.74s**	**0.05s (20x)**	1.18%	**0.42%**	1.00s	**0.74%**	0.66%	6.42s
KITTEN	106k	**1.13s**	**0.06s (22x)**	0.78%	**0.43%**	1.29s	**0.47%**	0.55%	11.18s
BIMBA	149k	**1.79s**	**0.09s (29x)**	1.92%	0.73%	2.62s	**0.63%**	**0.69%**	13.55s
APHRODITE	205k	**2.66s**	**0.12s (47x)**	1.20%	**0.46%**	5.58s	**0.58%**	0.59%	25.74s
LION	353k	**5.25s**	**0.24s (24x)**	1.92%	0.84%	10.92s	**0.68%**	**0.67%**	22.33s
RAMSES	1.6M	**63.4s**	**1.45s (68x)**	0.49%	**0.24%**	98.11s	**0.29%**	0.35%	268.87s

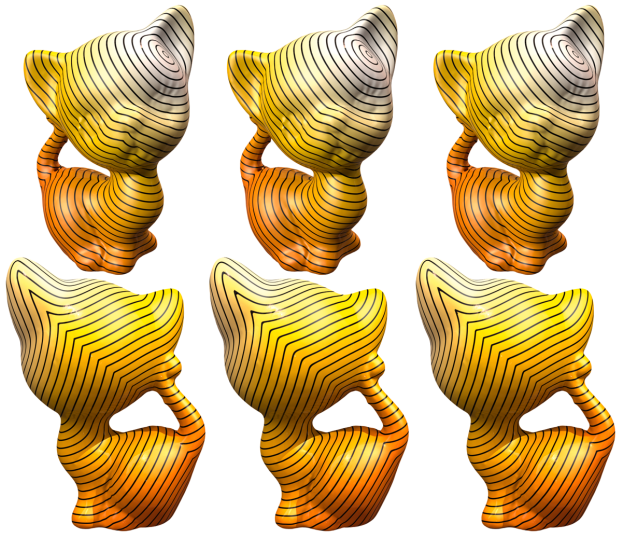

Fig. 14. Visual comparison of accuracy. *Left:* exact geodesic distance. Using default parameters, the heat method *(middle)* and fast marching (right) both produce results of comparable accuracy, here within less than 1% of the exact distance – see Table I for a more detailed comparison.
Kitten mesh courtesy AIM@Shape.

but cannot be used to obtain the true geometric distance. Overall, the heat method exhibits errors of the same order and magnitude as fast marching (at lower computational cost) and is therefore suitable in applications where fast marching is presently used.

The accuracy of the heat method depends on the particular choice of spatial discretization, and might be further improved by considering an alternative discrete Laplacian (see for instance [Belkin et al. 2009b; Hildebrandt and Polthier 2011]). In the case of fast marching, accuracy is determined by the choice of *update rule*. A number of highly accurate update rules have been developed for regular grids (*e.g.*, HJ WENO [Jiang and Peng 1997]), but fewer options are available on irregular domains such as triangle meshes, the predominant choice being the first-order update rule of Kimmel and Sethian [1998]. Finally, the approximate algorithm of Surazhsky *et al.* provides an interesting comparison since it tends to produce results more accurate than fast marching at a similar computational cost. However, one should be careful to note that accuracy is measured relative to the polyhedral distance rather than the smooth geodesic distance of the approximated surface (see [Surazhsky et al. 2005], Table 1). Similar to fast marching, Surazhsky's method does not take advantage of precomputation and therefore exhibits a significantly higher amortized cost than the heat method; it is also limited to triangle meshes.

[1] *Bunny mesh courtesy Stanford Computer Graphics Laboratory. Isis, Horse, Bibma, Lion, and Ramses meshes courtesy AIM@Shape. Aphrodite mesh courtesy Jotero GbR.*

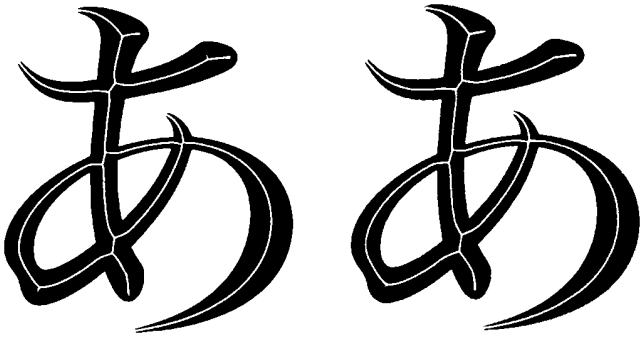

Fig. 15. Medial axis of the hiragana letter "a" extracted by thresholding second derivatives of the distance to the boundary. Left: fast marching. Right: heat method.

4.3 Robustness

Two factors contribute to the robustness of the heat method, namely (1) the use of an unconditionally stable implicit time-integration scheme and (2) formulation in terms of elliptic PDEs. Figure 16 verifies that the heat method continues to work well even on meshes that are poorly discretized or corrupted by a large amount of noise (here modeled as uniform Gaussian noise applied to the vertex coordinates). In this case we use a moderately large value of t to investigate the behavior of our smoothed distance; similar behavior is observed for small t values. Figure 17 illustrates the robustness of the method on a surface with many small holes as well as long sliver triangles.

Fig. 16. Tests of robustness. *Left:* our smoothed distance ($m = 10^4$) appears similar on meshes of different resolution. *Right:* even for meshes with severe noise *(top)* we recover a good approximation of the distance function on the original surface *(bottom, visualized on noise-free mesh)*.
Amphora mesh courtesy AIM@Shape.

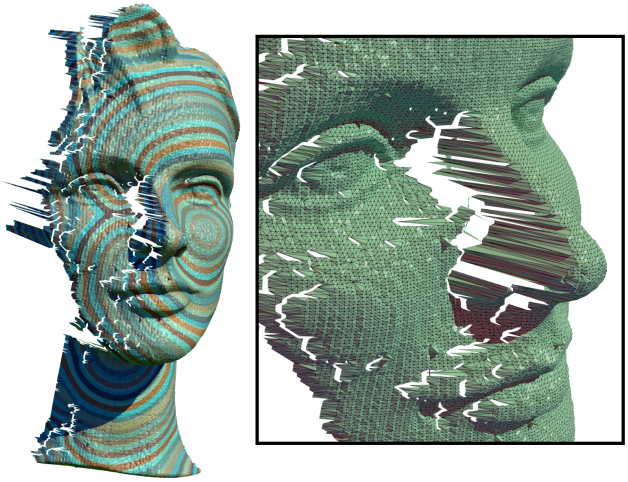

Fig. 17. Smoothed geodesic distance on an extremely poor triangulation with significant noise – note that small holes are essentially ignored. Also note good approximation of distance even along thin slivers in the nose.

5. CONCLUSION

The heat method is a simple, general method that can be easily incorporated into a broad class of algorithms. However, a great deal remains to be explored, including an investigation of alternative spatial discretizations. Further optimization of the parameter t also provides an avenue for future work (especially in the case of variable spacing), though one should note that the existing estimate already outperforms fast marching in terms of mean error (Table I). Another obvious question is whether a similar transformation can be applied to a larger class of Hamilton-Jacobi equations – for instance, a variable speed function might be incorporated by locally rescaling the metric. Finally, *weighted* distance computation might be achieved by simply rescaling the source data.

REFERENCES

Marc Alexa and Max Wardetzky. 2011. Discrete Laplacians on General Polygonal Meshes. *ACM Trans. Graph.* 30, 4 (2011), 102:1–102:10.

Mikhail Belkin, Jian Sun, and Yusu Wang. 2009a. Constructing Laplace operator from point clouds in R^d. In *ACM-SIAM Symp. Disc. Alg.*

Mikhail Belkin, Jian Sun, and Yusu Wang. 2009b. Discrete Laplace Operator for Meshed Surfaces. In *ACM-SIAM Symp. Disc. Alg.* 1031–1040.

D. Bommes and Leif Kobbelt. 2007. Accurate computation of geodesic distance fields for polygonal curves on triangle meshes. In *Proc. Workshop on Vision, Modeling, and Visualization (VMV)*. 151–160.

Mario Botsch, David Bommes, and Leif Kobbelt. 2005. Efficient linear system solvers for mesh processing. In *IMA Conference on the Mathematics of Surfaces*. Springer, 62–83.

Marcel Campen and Leif Kobbelt. 2011. Walking On Broken Mesh: Defect-Tolerant Geodesic Distances and Parameterizations. *Computer Graphics Forum* 30, 2 (2011), 623–632.

P. Chebotarev. 2011. The Walk Distances in Graphs. *ArXiv e-prints* (2011).

Yanqing Chen, Timothy A. Davis, William W. Hager, and Sivasankaran Rajamanickam. 2008. Algorithm 887: CHOLMOD, Supernodal Sparse Cholesky Factorization and Update/Downdate. *ACM Trans. Math. Softw.* 35, Article 22 (October 2008), 14 pages. Issue 3.

Ronald R. Coifman and Stephane Lafon. 2006. Diffusion maps. *Appl. Comput. Harmon. Anal.* 21 (2006), 5–30.

Mathieu Desbrun, Eva Kanso, and Yiying Tong. 2008. Discrete Differential Forms for Computational Modeling. In *Discrete Differential Geometry*. Oberwolfach Seminars, Vol. 38. Birkhäuser Verlag, 287–324.

Francois Fouss, Alain Pirotte, Jean-Michel Renders, and Marco Saerens. 2007. Random-Walk Computation of Similarities between Nodes of a Graph with Application to Collaborative Recommendation. *IEEE Trans. on Knowl. and Data Eng.* 19, 3 (2007), 355–369.

Klaus Hildebrandt and Konrad Polthier. 2011. On approximation of the Laplace-Beltrami operator and the Willmore energy of surfaces. *Comput. Graph. Forum* 30, 5 (2011), 1513–1520.

S. Hysing and S. Turek. 2005. The Eikonal Equation: Numerical Efficiency vs. Algorithmic Complexity. In *Proc. Algoritmy*. 22–31.

Guangshan Jiang and Danping Peng. 1997. Weighted ENO Schemes for Hamilton-Jacobi Equations. *SIAM J. Sci. Comput* 21 (1997), 2126–2143.

Ron Kimmel and J.A. Sethian. 1998. Fast Marching Methods on Triangulated Domains. *Proc. Nat. Acad. Sci.* 95 (1998), 8341–8435.

Yaron Lipman, Raif M. Rustamov, and Thomas A. Funkhouser. 2010. Biharmonic Distance. *ACM Trans. Graph.* 29, Article 27 (July 2010), 11 pages. Issue 3.

Yang Liu, Balakrishnan Prabhakaran, and Xiaohu Guo. 2012. Point-Based Manifold Harmonics. *IEEE Trans. Vis. Comp. Graph.* 18 (2012).

Chuanjiang Luo, Issam Safa, and Yusu Wang. 2009. Approximating Gradients for Meshes and Point Clouds via Diffusion Metric. *Comput. Graph. Forum* 28, 5 (2009), 1497–1508.

Richard MacNeal. 1949. *The Solution of Partial Differential Equations by means of Electrical Networks*. Ph.D. Dissertation. Caltech.

F. Memoli and G. Sapiro. 2001. Fast Computation of Weighted Distance Functions and Geodesics on Implicit Hyper-Surfaces. *Journal of Comp. Physics* 173 (2001), 730–764.

F. Memoli and G. Sapiro. 2005. Distance Functions and Geodesics on Submanifolds of $\mathbb{R}^d$ and Point Clouds. *SIAM J. Appl. Math.* 65, 4 (2005).

J. Mitchell, D. Mount, and C. Papadimitriou. 1987. The discrete geodesic problem. *SIAM J. of Computing* 16, 4 (1987), 647–668.

Andrew Nealen. 2004. *An As-Short-As-Possible Intro. to the MLS Method for Scattered Data Approximation and Interpolation*. Technical Report.

Robert Neel and Daniel Stroock. 2004. Analysis of the cut locus via the heat kernel. *Surveys in Differential Geometry* 9 (2004), 337–349.

James Norris. 1997. Heat Kernel Asymptotics and the Distance Function in Lipschitz Riemannian Manifolds. *Acta Math.* 179, 1 (1997), 79–103.

G. Peyré and L. D. Cohen. 2005. *Prog. in Nonlin. Diff. Eq. and Their Applications*. Vol. 63. Springer, Chapter Geodesic Computations for Fast and Accurate Surface Remeshing and Parameterization, 157–171.

Anand Rangarajan and Karthik Gurumoorthy. 2011. *A Fast Eikonal Equation Solver using the Schrödinger Wave Equation*. Technical Report REP-2011-512. CISE, University of Florida.

Raif Rustamov, Yaron Lipman, and Thomas Funkhouser. 2009. Interior Distance Using Barycentric Coordinates. *Computer Graphics Forum (Symposium on Geometry Processing)* 28, 5 (July 2009).

Phillip G. Schmitz and Lexing Ying. 2012. A fast direct solver for elliptic problems on general meshes in 2D. *J. Comput. Phys.* 231, 4 (2012).

G. Schwarz. 1995. *Hodge decomposition: a method for solving boundary value problems*. Springer.

J.A. Sethian. 1996. *Level Set Methods and Fast Marching Methods: Evolving Interfaces in Computational Geometry, Fluid Mechanics, Computer Vision and Materials Science*. Cambridge University Press.

Daniel A. Spielman and Shang-Hua Teng. 2004. Nearly-linear time algorithms for graph partitioning, graph sparsification, and solving linear systems. In *Proc. ACM Symp. Theory Comp. (STOC '04)*. ACM, 81–90.

Vitaly Surazhsky, Tatiana Surazhsky, Danil Kirsanov, Steven J. Gortler, and Hugues Hoppe. 2005. Fast exact and approximate geodesics on meshes. *ACM Trans. Graph.* 24 (2005), 553–560. Issue 3.

S. R. S. Varadhan. 1967. On the behavior of the fundamental solution of the heat equation with variable coefficients. *Communications on Pure and Applied Mathematics* 20, 2 (1967), 431–455.

Elena Villa. 2006. *Methods of Geometric Measure Theory in Stochastic Geometry*. Ph.D. Dissertation. Università degli Studi di Milano.

Max-K. von Renesse. 2004. Heat Kernel Comparison on Alexandrov Spaces with Curvature Bounded Below. *Potential Analysis* 21, 2 (2004).

Ofir Weber, Yohai S. Devir, Alexander M. Bronstein, Michael M. Bronstein, and Ron Kimmel. 2008. Parallel algorithms for approximation of distance maps on parametric surfaces. *ACM Trans. Graph.* 27, 4 (2008).

APPENDIX

A. A VARADHAN FORMULA FOR GRAPHS

LEMMA 1. *Let $G = (V, E)$ be the graph induced by nonzeros in any real symmetric matrix A, and consider the linear system*

$$(I - tA)u_t = \delta$$

where I is the identity, δ is a Kronecker delta at a source vertex $u \in V$, and $t > 0$ is a real parameter. Then generically

$$\boxed{\phi = \lim_{t \to 0} \frac{\log u_t}{\log t}}$$

*where $\phi \in \mathbb{N}_0^{|V|}$ is the **graph distance** (*i.e.*, number of edges) between each vertex $v \in V$ and the source vertex u.*

PROOF. Let σ be the operator norm of A. Then for $t < 1/\sigma$ the matrix $B := I - tA$ has an inverse and the solution u_t is given by the convergent Neumann series $\sum_{k=0}^{\infty} t^k A^k \delta$. Let $v \in V$ be a vertex n edges away from u, and consider the ratio $r_t := |s|/|s_0|$ where $s_0 := (t^n A^n \delta)_v$ is the first nonzero term in the sum and $s = (\sum_{k=n+1}^{\infty} t^k A^k \delta)_v$ is the sum of all remaining terms. Noting that $|s| \leq \sum_{k=n+1}^{\infty} t^k ||A^k \delta|| \leq \sum_{k=n+1}^{\infty} t^k \sigma^k$, we get

$$r_t \leq \frac{t^{n+1}\sigma^{n+1} \sum_{k=0}^{\infty} t^k \sigma^k}{t^n (A^n \delta)_v} = c \frac{t}{1 - t\sigma},$$

where the constant $c := \sigma^{n+1}/(A^n \delta)_v$ does not depend on t. We therefore have $\lim_{t \to 0} r_t = 0$, *i.e.*, only the first term s_0 is significant as t goes to zero. But $\log s_0 = n \log t + \log(A^n \delta)_v$ is dominated by the first term as t goes to zero, hence $\log(u_t)_v / \log t$ approaches the number of edges n. □

Numerical experiments such as those depicted in Figure 18 agree with this analysis. See also [Chebotarev 2011].

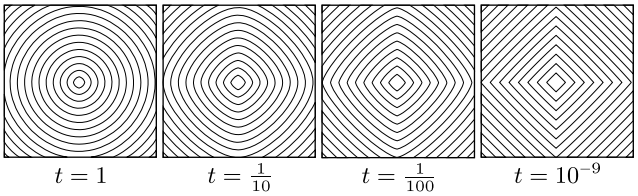

Fig. 18. Isolines of $\log u_t / \log t$ computed in exact arithmetic on a regular grid with unit spacing ($h = 1$). As predicted by Lemma 1, the solution approaches the combinatorial distance as t goes to zero.

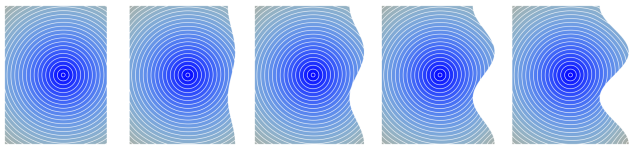

Fig. 19. Smoothed geodesic distance ($m = 1000$) using "averaged" boundary conditions. Notice that increasing geodesic curvature along the boundary does not strongly influence the behavior of the solution.

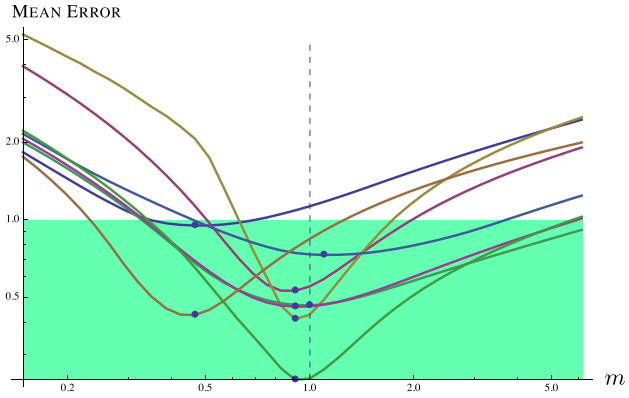

Fig. 20. Mean percent error as a function of m, where $t = mh^2$. Each curve corresponds to a data set from Table I. Notice that in most examples $m = 1$ (dashed line) is close to the optimal parameter value (blue dots) and yields mean error below 1%.

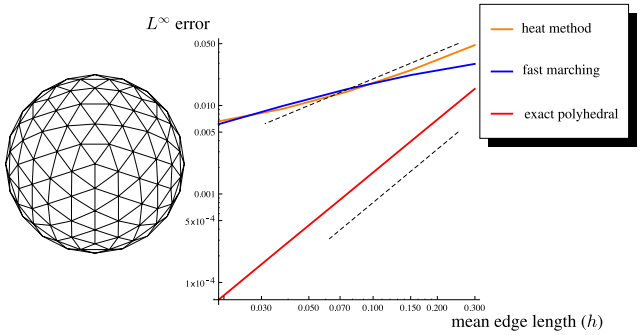

Fig. 21. L^∞ convergence of distance functions on the unit sphere with respect to mean edge length. As a baseline for comparison, we use the exact distance function $\phi(x, y) = \cos^{-1}(x \cdot y)$. Linear and quadratic convergence are plotted as dashed lines for reference; note that even the exact polyhedral distance converges only quadratically.

ACKNOWLEDGMENTS

This work was funded by a Google PhD Fellowship and a grant from the Fraunhofer Gesellschaft. Thanks to Michael Herrmann for inspiring discussions, and Ulrich Pinkall for discussions about Lemma 1. Meshes are provided courtesy of the Stanford Computer Graphics Laboratory, the AIM@Shape Repository, Luxology LLC, and Jotero GbR (`http://www.evolution-of-genius.de/`).

Received September 2012; accepted March 2013

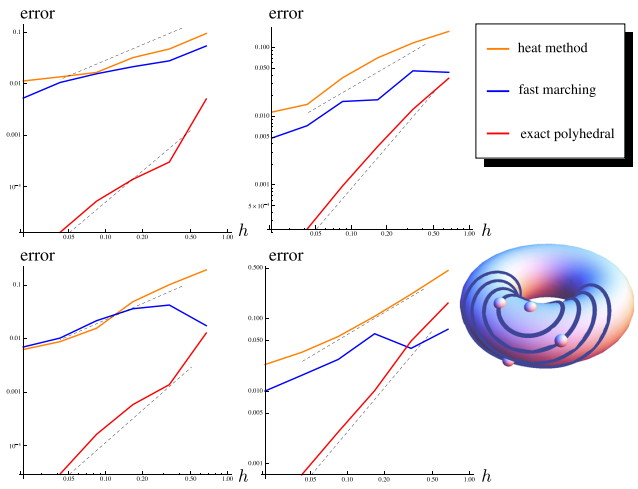

Fig. 22. Convergence of geodesic distance on the torus at four different test points. Error is the absolute value of the difference between the numerical value and the exact (smooth) distance; linear and quadratic convergence are plotted as dashed lines for reference. *Right:* test points visualized on the torus; dark blue lines are geodesic circles computed via Clairaut's relation.

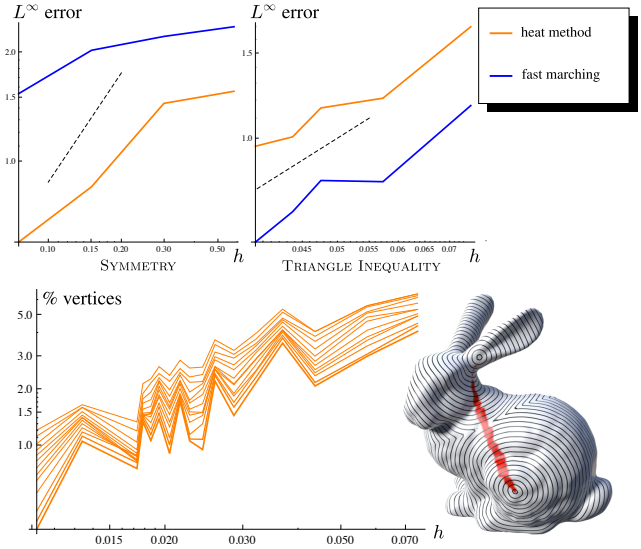

Fig. 23. Fast marching and the heat method both exhibit small violations of metric properties such as symmetry *(top left)* and the triangle inequality *(top right)* that vanish under refinement – we plot the worst violation among all pairs or triples of vertices (respectively) as a percent of mesh diameter. Dashed lines plot linear convergence. *Bottom right:* the triangle inequality is violated only for vertices along a geodesic between two distinguished points (in **red**), since the corresponding geodesic triangles are nearly degenerate. *Bottom left:* percent of red vertices as a function of h – each curve represents a different value of m sampled from the range $[1, 100]$.

Bunny mesh courtesy Stanford Computer Graphics Laboratory.